

Todo list

Describe scintillation detector better. Read William Tomkin's thesis, page 8.	6
Over what energy range did COS-B observe photons?	8
Figure out if EGRET was first to detect a PWNe (crab nebula. EGRET analysis: http://adsabs.harvard.edu/abs/1993ApJ...409..697N COS-B Analysis: http://adsabs.harvard.edu/abs/1987A%26A...174...85C	9
How many γ -rays the Energetic Gamma Ray Experiment Telescope (EGRET) detect?	9
How many pulsars did EGRET detect?	9
Short description of the history of TeV astronomy	9
What is the LAT effective area?	9
Make note of "Air force had early warning of pulsars" paper	10
First gamma-ray detection	11
When was the PSR, PWN connection made	11
3 Types of pulsars (rotationally powered pulsars, magnetars, accretion powered pulsars,	15
Find a plot of a rotating pulsar. The simplest rotating dipole model	16
Discuss uniform dipole model	17
Discuss pulsar evolution "The Evolution and Structure of Pulsar Wind Nebulae" – Bryan M. Gaensler and Patrick O. Slane	18
Describe Mattana's work on pulsar wind nebulae (PWNe): "On the evolution of the Gamma- and X-ray luminosities of Pulsar Wind Nebulae"	18
Include discussion of modeling, if time permitting	18
Describe Catalog	19

Dig up HESS reference of HESS J1514-59.	20
what section discusses energy dependent psf?	25
What are the benefits of maximum likelihood	26
Describe Wilk's Theorem and it's application to parameter error estimation .	26
WHAT SECTION DESCRIBES EXTENDED SOURCE PDFs	28
FINISH DISCUSSION	28
Discuss how diffuse background is more complicated and requires a mapcube.	28
LINK TO arXiv:1206.1896 for MORE THOUROUGH DISCUSSION OF EF- FECTIVE AREA	29
DISCUSS HOW EFFECTIVE AREA IS A FUNCTION OF DIFFERENT THINGS	29
What is the range of the integrals	29
BETTER DISCUSSION OF PSF OF THE LAT, WHAT ITS SCALE IS... .	30
Why discard time dispersion	30
WRITE ENERGY DISPERSION AS A DELTA FUNCTION	30
FINISH	31
Figure out how the θ dependence of the IRFs factors into this calculation . . .	31
Write Section or Perform simple MC Simulation to demonstrate significance of detection	32
What would make good future work. Something about CTA population study, something about improved modeling like HESS J1825, something about better PSF	40

OBSERVATIONS OF PWNE WITH THE FERMI GAMMA-RAY
SPACE TELESCOPE

A DISSERTATION
SUBMITTED TO THE DEPARTMENT OF PHYSICS
AND THE COMMITTEE ON GRADUATE STUDIES
OF STANFORD UNIVERSITY
IN PARTIAL FULFILLMENT OF THE REQUIREMENTS
FOR THE DEGREE OF
DOCTOR OF PHILOSOPHY

Joshua Jeremy Lande

February 2013

© Copyright by Joshua Jeremy Lande 2013
All Rights Reserved

I certify that I have read this dissertation and that, in my opinion, it is fully adequate in scope and quality as a dissertation for the degree of Doctor of Philosophy.

(Stefan Funk) Principal Adviser

I certify that I have read this dissertation and that, in my opinion, it is fully adequate in scope and quality as a dissertation for the degree of Doctor of Philosophy.

(Elliott Bloom)

I certify that I have read this dissertation and that, in my opinion, it is fully adequate in scope and quality as a dissertation for the degree of Doctor of Philosophy.

(Roger Romani)

Approved for the University Committee on Graduate Studies

Abstract

Two things fill the mind with ever-increasing wonder and awe, the more often and the more intensely the mind of thought is drawn to them: the starry heavens above me and the moral law within me.” – Immanuel Kant

The launch of the *Fermi* Gamma-ray space telescope in 2008 offered an unprecedented view into the γ -ray sky.

All the things we can learn with the the Large Area Telescope (LAT)

Development of a new analysis method for studying spatially-extended PWNs using `pointlike`.

A monte-carlo validation of the analysis method.

Search for new spatially-extended sources with the LAT.

Observations of PWNs in the off-peak region of LAT detected pulsars.

Search for PWNs counterparts to TeV sources.

Using the population of PWNs to understand the radiation mechanism of PWNs.

Acknowledgement

Acknowledge the educational institutes which taught me physics: My high school HB Woodlawn, my undergraduate institution Marlboro College, and my Stanford University.

First, I would like to acknowledge those mentors who inspired me to get a PhD.

- Mark Dodge, my high school physics teacher.
- Ron Turner, my internship adviser at Analytic Services (ANSER) during the GWU Science and Engineering Apprentice Program (SEAP)
- Anthony Tyson at UC Davis for my SULI Internship
- Apurva Mehta and Sam Webb sam Web at SLAC SULI Internship.

During my PhD I was helped by an almost overwhelminlgy large number of people in the LAT collaboration.

People at Stanford/SLAC: Stefan Funk, Elliott Bloom, Markus Ackermann, Tobias Jogler, Junichiro Katsuta, Yasunobu Uchiyama, Seth Digel, James Chiang

pointlike collaborators: Matthew Kerr, Toby Burnett, Eric Wallace, Marshall Roth

Pulsar Collaborators: David Smith, Matthew Kerr, Peter den Hartog, Tyrel Johnson, Damien Parent, Ozlem Celik

Careful review of text: Jean Ballet, Johann Cohen-Tanugi

I would like to thank the PWNs people Thank the people in Bordeaux: Marianne Lemoine-Goumard, Romain Rousseau, and Marie-Hélène Grondin

Fermi SLAC Grad Students: Keith Bechtol, Alex Drlica-Wagner, Alice Allafort, Herman Lee Yvonne Edmonds, Bijan Berenji, Ping Wang, Warit Mitthumsiri

Joanne Bogart, Heather Kelly, Richard Dubois, Renata Dart, Stuart Marshall, and Glenn Morris for putting up with my computer problems.

Martha Siegel, Chris Hall, Ziba Mahdavi, awesome SLAC administrators. Maria Frank, Elva Carbajal, and Violet Catindig , awesome Stanford administrators.

Additional Astro Stanford Graduate Students: Helen Craig, Michael Shaw, Adam Van Etten, Kyle Watters

Additonal Graduate Students at Stanford: Dan Riley, Joel Frederico, Ahmed Ismail, Joshua Cogan, Kunal Sahasrabuddhe,

Contents

Abstract	iv
Acknowledgement	v
1 Overview	3
2 Gamma-ray Astrophysics	4
2.1 Astronomy and the Atmosphere	4
2.2 The History of Gamma-ray Astrophysics	5
2.3 The <i>Fermi</i> Gamma-ray Space Telescope	10
2.3.1 The Tracker	10
2.3.2 The Calorimeter	10
2.3.3 Anti-Coincidence Detector	10
2.3.4 Gamma-ray Burst Monitor	10
2.4 Astrophysical Sources of Gamma-rays	10
2.4.1 Pulsars	10
2.4.2 Pulsar Wind Nebulae	11
2.5 Radiation Processes in Gamma-ray Astrophysics	14
2.5.1 Synchrotron	14
2.5.2 Inverse Compton	14
2.5.3 Bremsstrahlung	14
2.5.4 π^0 Decay	14
2.6 The Pulsar/Pulsar Wind Nebula System	14
2.6.1 Neutron Star Formation	14

2.6.2	Pulsar Evolution	16
2.6.3	Pulsar Magnetosphere	18
2.6.4	Pulsar Wind Nebulae	18
2.7	Modeling the Galactic Diffuse and Isotropic Gamma-ray Background	18
2.8	Sources Detected by the Fermi The Large Area Telescope	19
2.8.1	The second <i>Fermi</i> catalog	19
2.8.2	The second <i>Fermi</i> pulsar catalog	20
2.8.3	Pulsar wind nebula Detected by the The Large Area Telescope	20
3	Maximum-likelihood analysis of LAT data	24
3.1	Motivations for Maximum-Likelihood Analysis of Gamma-ray Data .	25
3.2	Description of Maximum-Likelihood Analysis	26
3.3	Defining a Model of the Sources in the Sky	26
3.4	The LAT Instrument Response Functions	29
3.5	Binned Maximum-Likelihood of LAT Data with the Science Tools . .	31
3.6	The Alternate Maximum-Likelihood Package <code>pointlike</code>	33
4	Analysis of Spatially Extended LAT Sources	34
4.1	Analysis Method	34
4.2	Validation of the TS Distribution	34
4.3	Extended Source Detection Threshold	34
4.4	Testing Against Source Confusion	34
4.5	Test of 2LAC Sources	34
4.6	Systematic Errors on Extension	34
5	Search for Spatially-extended LAT Sources	35
5.1	Extended Source Search Method	35
5.2	New Extended Sources	35
5.3	Discussion	35
6	Search for Pulsar Wind Nebulae associated with Gamma-loud Pulsars	36

6.1	Off-peak Phase Selection	36
6.2	Off-peak Analysis Method	36
6.3	Off-peak Results	36
6.4	Off-Peak Individual Source Discussion	36
7	Search for Pulsar Wind Nebulae associated with TeV Pulsars	37
7.1	List of Candidates	37
7.2	Analysis Method	37
7.3	Sources Detected	37
8	Search for Pulsar Wind Nebulae associated with High \dot{E} Pulsars	38
9	Population Study of The Large Area Telescope (LAT)-detected Pulsar wind nebula (PWN)	39
10	Future Work (or Outlook)??	40

List of Tables

List of Figures

2.1	Transparency of the atmosphere of the earth to photons of varying wavelenthts. This figure is from Carroll & Ostlie (2006)	5
2.2	The position of all 621 cosmic γ -rays detected by the Third Orbiting Solar Observatory (OSO-3). This figure is from Kraushaar et al. (1972).	7
2.3	A map of the sources observed by COS-B. The filled circles represent brighter sources. The unshaded region corresponds to the parts of the sky observed by COS-B. This figure is from Swanenburg et al. (1981).	9
2.4	The Orion plate from Bevis' book <i>Uranographia Britannica</i> . The Crab nebula can be found on the horn of Taurus the Bull on the top of the figure and the source is marked by a cloudy symbol. This figure was reproduced from Ashworth (1981).	22
2.5	The simplest model of a puslar. Figure from (Carroll & Ostlie 2006).	23

List of Acronyms

2CG the second COS-B catalog. 8

2FGL the second *Fermi* catalog. viii, 19, 25

2PC the second *Fermi* pulsar catalog. viii, 20

ACD Anti-Coincidence Detector. vii, 10

BPL broken-power law. 27

CGRO the Compton Gamma Ray Observatory. 9

CGS the Centimetre-Gram-Second System of Units. 27, 28

ECPL exponentially-cutoff power law. 27, 28

EGRET the Energetic Gamma Ray Experiment Telescope. 1, 8, 9

ESA the European Space Agency. 8

FWHM full width at half maximum. 7

GBM Gamma-ray Burst Monitor. vii, 10

IC inverse Compton. vii, 6, 14

LAT the Large Area Telescope. iv, v, viii, ix, 10, 19, 20, 35, 39

MIT the Massachusetts Institute of Technology. 6, 11

NASA the National Aeronautics and Space Administration. 8

NRL the Naval Research Laboratory. 11

OSO-3 the Third Orbiting Solar Observatory. xi, 6–8, 19

PL power law. 27, 28

PWN pulsar wind nebula. iv, v, viii, ix, 1, 6, 11, 14, 16, 18, 20, 39

SA solid angle. 29, 30

SAS-2 the second Small Astronomy Satellite. 7, 8

SNR supernova remnant. 28

Chapter 1

Overview

In Chapter 2, we discuss the history of γ -ray astrophysics, ...

Chapter 2

Gamma-ray Astrophysics

2.1 Astronomy and the Atmosphere

Humans surely have, since the very beginning, stared into space and contemplated its brilliance. Stone circles in the Nabta Playa in Egypt are likely the first observed astronomical observatory and are believed to have acted as a prehistoric calendar. Dating back to the 5th century BC, they are 1,000 years older than stonehenge (McK Mahille et al. 2007).

Astronomy has historically been almost entirely concerned with studying the photons that arrive from outer space. Because of their charge neutrality, photons are not deflected by intergalactic electric and magnetic fields and therefore point back to the objects emitting them.

Historically, the field of astronomy concerned the study of visible light. The reason for this is visible light is not significantly absorbed in the atmosphere. In addition to the visible spectrum, radio waves, some energies of infrared radiation, and long-wavelength ultraviolet radiation can be measured from the ground. Figure 2.1 shows the transparency of the atmosphere of the earth to photons of different wavelengths.

Slowly, over time, astronomers expanded their view across the electromagnetic spectrum. First, the astronomical observations were made from the ground. Infrared radiation from the sun was first observed by William Herschel in 1800. Herschel

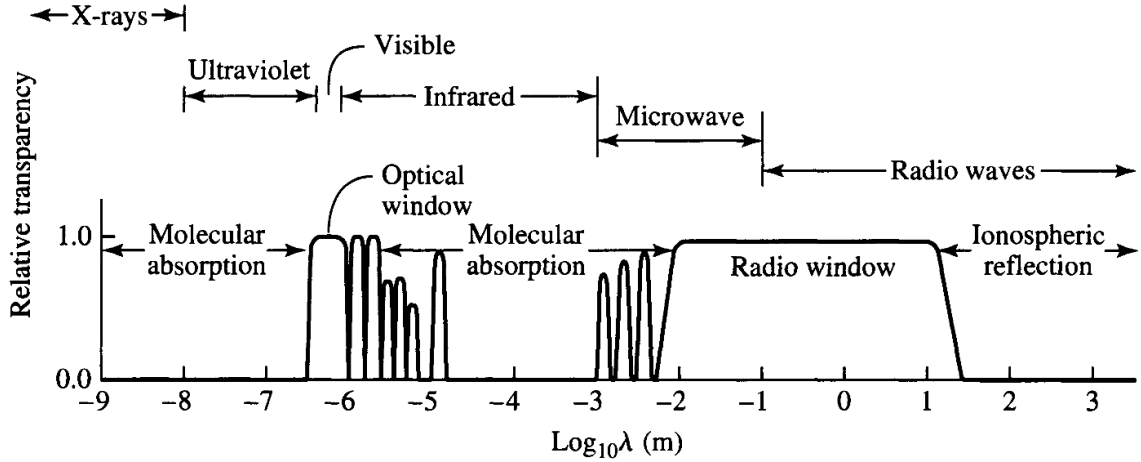


Figure 2.1: Transparency of the atmosphere of the earth to photons of varying wavelenths. This figure is from Carroll & Ostlie (2006)

measured this infrared radiation by measuring the temperature of sunlight through a prisim and extending the measurement past the red part of the spectrum (Herschel 1800). The first extraterrestrial source of radio waves was detected by Jansky in 1933. Jansky, a radio engineer at Bell labs, was studying the origins of radio interference when he detected radio emission towards the center of our galaxy. (Jansky 1933).

The expansion of the astronomical fronteire to other wavelenths required the develpoment of rockets and sattelites in the 20th ceuntry. The first ultraviolet observation of the sun was performed in 1946 from a captured V-2 rocket (Baum et al. 1946). Observations of solar x-rays were also first carried out on a captured V-2 Rocket in 1949 (Burnight 1949).

2.2 The History of Gamma-ray Astrophysics

It was only natural to wonder about photons with even higher energies. These higher energy photons must come from more extreme processes in space.

As is common in the field of physics, the prediction of the detection of cosmic γ -rays far proceded their discovery. Feenberg & Primakoff (1948) theorized that

the interaction of starlight with cosmic rays could produce γ -rays through inverse Compton (IC) upscattering. Following the discovery of the neutral pion in 1949, Hayakawa (1952) predicted that γ -ray emission could be observed from the decay of neutral pions when cosmic rays interacted with interstellar matter. And in the same year, Hutchinson (1952) discussed the bremsstrahlung radiation of cosmic-ray electrons. Morrison (1958) first predicted the detection of several sources of γ -rays including solar flares, pulsar wind nebulae (PWNe), and active galaxies.

Attempts were made in the 1940s and 1950s to determine the composition of cosmic rays using balloon-based experiments. See, for example Critchfield et al. (1952) and Hulsizer & Rossi (1948). But the attempt to observe cosmic γ -rays was hampered by the strong background of atmospheric albedo γ -rays.

The first space-based γ -ray detector was Explorer XI Kraushaar et al. (1965). It was developed at the Massachusetts Institute of Technology (MIT) under the direction of William L. Kraushaar. It employed a sandwich scintillator and a Cherenkov counter to direct the position and energy of incoming γ -rays and was surrounded by a plastic anticoincidence scintillation counter. The sandwich detector operated in the energy range for $E > 100$ MeV. It had an area of $\sim 45\text{cm}^2$ but an effective area of only $\sim 7\text{cm}^2$, corresponding to a detector efficiency of $\sim 15\%$.

It was launched on board Explorer XI on April 27, 1961. The instrument was in operation for 7 months, but only 141 hours of data were of acceptable quality. Using these observations, Explorer XI observed 31 γ -rays and, because the distribution a distribution of these γ -rays was consistent with being isotropic, the experiment could not firmly identify the γ -rays as being cosmic in nature.

Describe scintillation detector better. Read William Tomkin's thesis, page 8.

The first definitive detection of γ -ray came in 1962 by an experiment on the Ranger 3 moon probe (Arnold et al. 1962). It detected an isotropic flux of γ -rays in the 0.5 MeV to 2.1 MeV energy range.

The Third Orbiting Solar Observatory (OSO-3), also developed by Kraushaar, followed Explorer XI as the next major astrophysical γ -ray detector Kraushaar et al. (1972). OSO-3 allowed the on board γ -ray detected to have an improved weight,

power, telemetry, and exposure, creating a more sensitive experiment. The experiment operated in the energy range from 50 MeV to ~ 400 MeV, had an effective area $\sim 9 \text{ cm}^2$, and had an angular resolution of $\sim 24^\circ$ at its full width at half maximum (FWHM).

It was launched on March 8, 1967 and operated for 16 months, measuring 621 cosmic γ -rays. The most important result of the experiment was to measure a strong anisotropy in the distribution of the γ -rays with a strong clustering of γ -rays towards the Galactic plane. Figure 2.2 shows a skymap of these γ -rays. This experiment confirmed both a Galactic component to the γ -ray sky as well as an additional isotropic component, hypothesised to be extragalactic in origin.

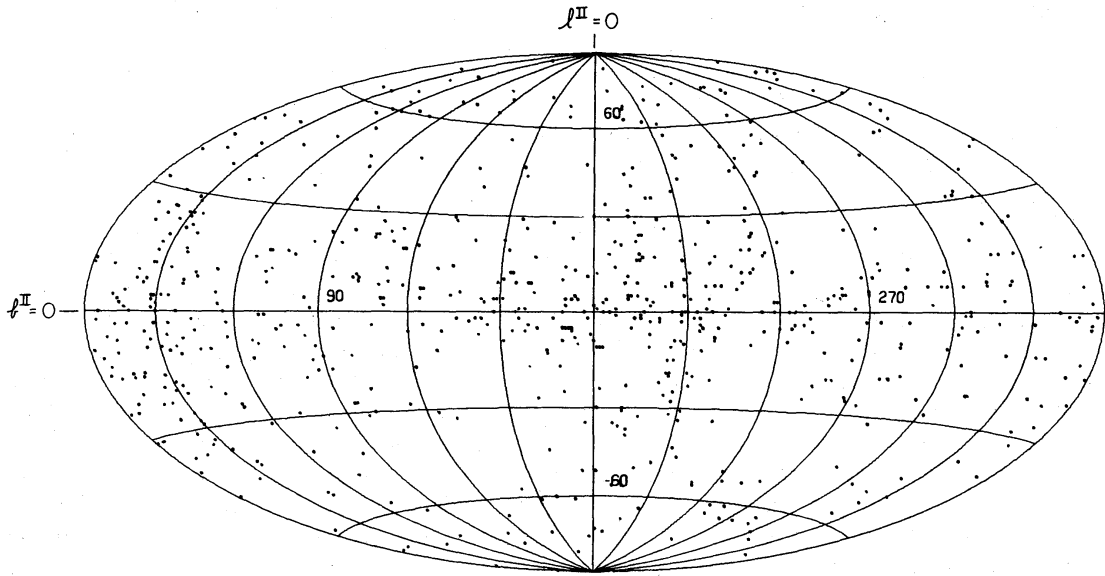


Figure 2.2: The position of all 621 cosmic γ -rays detected by OSO-3. This figure is from Kraushaar et al. (1972).

The major discovery by OSO-3 was confirmed by a balloon-based γ -ray detector in 1970 (Kniffen & Fichtel 1970). In the following year, the first γ -ray pulsar (the Crab) was detected by another balloon-based detector Browning et al. (1971).

The next major advancement in γ -ray astronomy came the second Small Astronomy Satellite (SAS-2) and COS-B.

SAS-2 was a dedicated γ -ray detector launched by the National Aeronautics and Space Administration (NASA) in November 15, 1972. SAS-2 was Fichtel et al. (1975). It improved upon OSO-3 by incorporating a spark chamber and having an overall larger size. The size of the active area of the detector was 640 cm^2 and the experiment had a much improved effective area of $\sim 115 \text{ cm}^2$. The spark chamber allowed for a separate measurement of the electron and positron tracks, which allowed for improved directional reconstruction of the incident γ -ray. SAS-2 had a PSF $\sim 5^\circ$ at 30 MeV and $\sim 1^\circ$ at 1 GeV.

SAS-2 collected data for over 6 months before a power supply failure ended data collection. SAS-2 Observed over 8,000 γ -ray photons covering $\sim 55\%$ of the sky including most of the Galactic plane. SAS-2 discovered strong emission along the Galactic plane and particularly towards the Galactic center. It also discovered pulsations from the Crab (Fichtel et al. 1975) and Vela pulsar (Thompson et al. 1977b). In addition, SAS-2 discovered Geminga, the first γ -ray source with no compelling multiwavelength counterpart (Thompson et al. 1977a). Geminga was eventually discovered to be a pulsar by the Energetic Gamma Ray Experiment Telescope (EGRET) (Bertsch et al. 1992) and retroactively by SAS-2 (Mattox et al. 1992).

on August 9, 1975, the European Space Agency (ESA) launched COS-B, a γ -ray detector similar to SAS-2. COS-B included a spark chamber but improved upon the design of SAS-2 by including a calorimeter below the spark chamber which improved the energy resolution to $< 100\%$ for energies $\sim 3 \text{ GeV}$ (Bignami et al. 1975). COS-B has a comparable effective area to SAS-2: $\sim 50 \text{ cm}^2$ at $\sim 400 \text{ MeV}$ (Bignami et al. 1975).

Over what energy range did COS-B observe photons?

COS-B operated successfully for over 6 years and produced the first detailed catalog of the γ -ray sky. In total, COS-B observed $\sim 80,000$ photons Mayer-Hasselwander et al. (1982). The second COS-B catalog (2CG) detailed the detection 25 γ -ray sources for $E > 100 \text{ MeV}$ (Swanenburg et al. 1981). Figure 2.2 shows a map of these sources. Of these sources, the vast majority lay along the galactic plane and could not be positively identified with sources observed at other wavelengths. In addition, COS-B observed the first ever extragalactic γ -ray source, (3C273, Swanenburg et al. 1978).

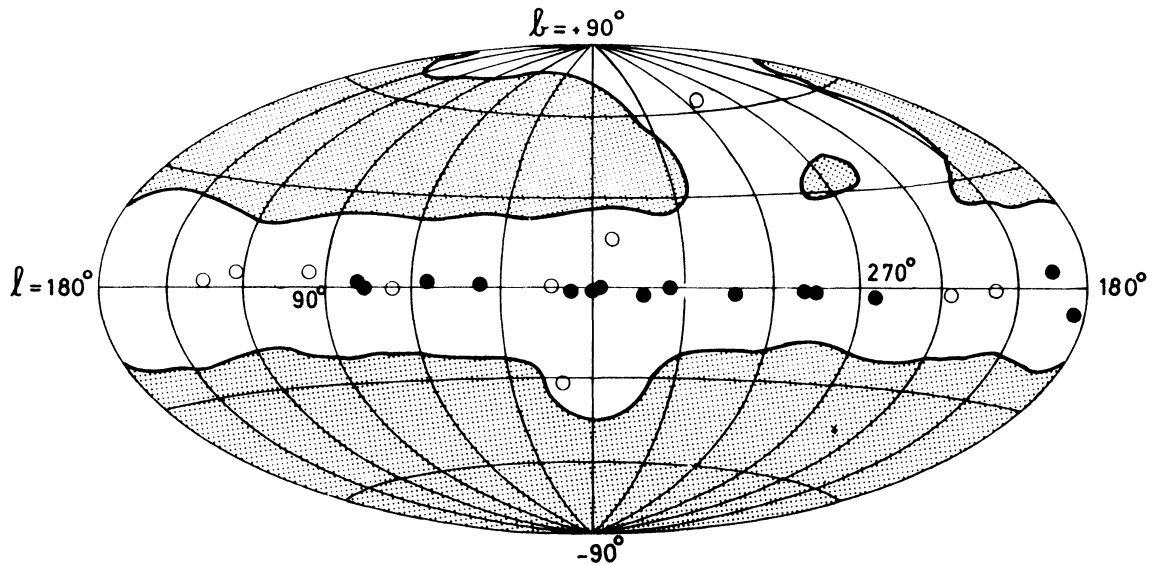


Figure 2.3: A map of the sources observed by COS-B. The filled circles represent brighter sources. The unshaded region corresponds to the parts of the sky observed by COS-B. This figure is from Swanenburg et al. (1981).

EGRET on board the Compton Gamma Ray Observatory (CGRO)

Figure out of EGRET was first to detect a PWNe (crab nebula. EGRET analysis: <http://adsabs.harvard.edu/abs/1993ApJ...409..697N> COS-B Analysis: <http://adsabs.harvard.edu/abs/1987A%26A...174...85C>

How many γ -rays EGRET detect?

How many pulsars did EGRET detect?

- AGILE

- *Fermi*

- Short description of the history of TeV astronomy

- A detailed description of *Fermi* detector will be presented in Section 2.3.4.

- The major source classes detected by *Fermi* will be presented in Section 2.8

The principles of the detector will be described in Section 2.3.4.

What is the LAT effective area?

2.3 The *Fermi* Gamma-ray Space Telescope

The Large Area Telescope (LAT) is a pair-production telescope

2.3.1 The Tracker

2.3.2 The Calorimeter

2.3.3 Anti-Coincidence Detector

The Anti-Coincidence Detector (ACD) is ...

2.3.4 Gamma-ray Burst Monitor

2.4 Astrophysical Sources of Gamma-rays

2.4.1 Pulsars

Pulsars were first discovered in 1967 by Jocelyn Bell Burnell and Antony Hewish (Hewish et al. 1968). They had constructed a radio telescope that used interplanetary scintillation with the intention of observing quasars. In the process, they detected a source with a periodicity of 1.3 s.

Make note of “Air force had early warning of pulsars” paper

Even before the discovery, Pacini (1967) had predicted the existence of neutron stars. Shortly following the 1967 discovery, Gold (1968) and Pacini (1968) argued that the observed pulsar was a rotating neutron star.

The discovery of many more pulsars came quickly. In 1968, and the Vela pulsar (Large et al. 1968) and the Crab pulsar (Staelin & Reifenstein 1968) were discovered.

The first pulsar observed at optical frequencies was the Crab, discovered in 1969 shortly after its radio discovery (Cocke et al. 1969). In the same year, the first X-ray

pulsations were discovered from the same source. At the time, there were no space-based X-ray observatories, so observations had to be performed from rockets. The discovery was carried out almost concurrently by a group at the Naval Research Laboratory (NRL) (Fritz et al. 1969) and at MIT (Bradt et al. 1969). Using proportional counters, these experiments showed that the pulsed emission from the Crab extended to X-ray energies and that, for this source, the X-rays emission was a factor > 100 more energetic than the observed visible emission.

- For Crab describe spin down?: “and these pulsations were then shown to be slowing down at a rate of 36 ns per day (Richards & Comella 1969).” – Gaensler & Slane (2006)

As was discussed in Section 2.2, γ -ray emission from the Crab was detected only 2 years later (Browning et al. 1971).

ATNF catalog?

- “There are currently more than 1,800 pulsars in the ATNF on-line catalog [Manchester et al., 2005], with rotation periods in the range 0.0016-12 seconds (Figure 3.1) and derived spin down luminosities in the range XXX - XXX erg/s.” – dalton_2011_identification-gamma-ray

EGRET pulsars?

The state of the art in γ -ray detection of pulsars will be included in an upcoming publication. 2PC: Section 2.8.2

When was the PSR, PWN connection made

First
gamma-
ray
detection

2.4.2 Pulsar Wind Nebulae

A PWN is a diffuse nebula of shocked relativistic particles. A PWNs surrounds and is powered by an accompanying pulsar. PWNs have been observed long before the discovery of pulsars, but the pulsar/PWN connection could not be made until after the detection of pulsars.

The most famous PWNs is the Crab nebula, associated with the Crab pulsar.

- Chinese SN observations of Crab Nebulae: (p128 of “The Crab Nebula: An Astrophysical Chimera”) “It was probably also recorded by Anasazi Indian artists (in present-day Arizona and New Mexico), as findings in Navaho Canyon and White Mesa (both Arizona) as well as in the Chaco Canyon National Park (New Mexico) indicate; there’s a review of the research on the Chaco Canyon Anasazi art online. In addition, Ralph R. Robbins of the University of Texas has found Mimbres Indian art from New Mexico, possibly depicting the supernova.”
– <http://messier.seds.org/m/m001.html>

It was discovered in 1731 by physician and amateur astronomer John Bevis. This source was going to be published in his sky atlas *Uranographia Britannica*, but the work was never published because his published filed for bankruptcy in 1750. Figure 2.4.2 shows Beavis’ plate containing the Crab nebula. A detailed history of John Bevis’ work can be found in Ashworth (1981).

- Crab Nebulae is M1 in Charles Messier’s catalog 1758 (p128 of “The Crab Nebula: An Astrophysical Chimera”)
- Connection to 1054: “Lundmark (1921) suggested a connection between the Crab Nebula and the event of 1054 AD” (p128 of “The Crab Nebula: An Astrophysical Chimera”) “The Crab Nebula (Fig. 1) is almost certainly associated with a supernova (SN) explosion observed in 1054 CE (Stephenson & Green 2002, and references therein).” – “The Evolution and Structure of Pulsar Wind Nebulae” Bryan M. Gaensler and Patrick O. Slane
- “The same year, J.C. Duncan of Mt. Wilson Observatory compared photographic plates taken 11.5 years apart, and found that the Crab Nebula was expanding at an average of about 0.2” per year; backtracing of this motion showed that this expansion must have begun about 900 years ago (Duncan 1921). Also the same year, Knut Lundmark noted the proximity of the nebula to the 1054 supernova (Lundmark 1921).” – <http://messier.seds.org/m/m001.html>
“In 1942, based on investigations with the 100-inch Hooker telescope on Mt. Wilson, Walter Baade computed a more accurate figure of 760 years ago from

the expansion, which yields a starting date around 1180 (Baade 1942); later investigations improved this value to about 1140. The actual 1054 occurrence of the supernova shows that the expansion must have been accelerated.” – <http://messier.seds.org/m/m001.html>

- “but it was not until 1942 that Duyvendak (1942) and Mayall & Oort (1942) presented complete studies of modern observations of the expanding nebula and of the early Chinese records. It was this work that established unambiguously that the Crab is the remnant of SN1054.” (p128 of “The Crab Nebula: An Astrophysical Chimera”)
- “1949, the Crab nebula was identified as a strong source of radio radiation (Bolton et.al. 1949), discovered 1948 named and listed as Taurus A (Bolton 1948), and later as 3C 144.” - <http://messier.seds.org/m/m001.html>
- Synchrotron emission hypothesis: “while the inner, blueish nebula emits continuous light consisting of highly polarised so-called synchrotron radiation, which is emitted by high-energy (fast moving) electrons in a strong magnetic field. This explanation was first proposed by the Soviet astronomer J. Shklovsky (1953) and supported by observations of Jan H. Oort and T. Walraven (1956).” – <http://messier.seds.org/m/m001.html>
- “X-rays from this object were detected in April 1963 with a high-altitude rocket of type Aerobee with an X-ray detector developed at the Naval Research Laboratory; the X-ray source was named Taurus X-1. Measurements during lunar occultations of the Crab Nebula on July 5, 1964, and repeated in 1974 and 1975, demonstrated that the X-rays come from a region at least 2 arc minutes in size, and the energy emitted in X-rays by the Crab nebula is about 100 times more than that emitted in the visual light” – <http://messier.seds.org/m/m001.html>
- Association of Crab pulsar with Crab nebulae were discussed in (Staelin & Reifenstein 1968).
- TEV observations of Crab. brightest source in the sky...

- Now many radio, x-ray PWNe. Count from PWN catalog: <http://www.physics.mcgill.ca/pulsar/pwnecat.html> “Observations over the last several decades have identified 40 to 50 further sources, in both our own Galaxy and in the Magellanic Clouds, with properties similar to those of the Crab Nebula (Green 2004; Kaspi, Roberts & Harding 2006)” – Gaensler & Slane (2006)
- How many TeV PWNe in TeVCat? <http://tevcat.uchicago.edu/> (31 by my preliminary count)

2.5 Radiation Processes in Gamma-ray Astrophysics

- The non-thermal radiation processes typical in astrophysics are most commonly

2.5.1 Synchrotron

2.5.2 Inverse Compton

IC emission is ...

IC

2.5.3 Bremsstrahlung

2.5.4 π^0 Decay

2.6 The Pulsar/Pulsar Wind Nebula System

2.6.1 Neutron Star Formation

As was discussed in Section 2.4, pulsars, PWNe, and supernova remnants are all the end products of supernovas. When a star undergoes a supernova, the ejecta forms a supernova remnant. If the remaining stellar core has a mass above the Chandrasekhar limit, then the core’s electron degeneracy pressure cannot counteract

the core's gravitational force and the core will collapse into a neutron star. The Chandrasekhar mass limit can be approximated as (Chandrasekhar 1931)

$$M_{\text{Ch}} \approx \frac{3\sqrt{2}\pi}{8} \left(\frac{\hbar c}{G} \right)^{3/2} \left[\left(\frac{Z}{A} \right) \frac{1}{m_{\text{H}}^2} \right] \quad (2.1)$$

where \hbar is the reduced Planck constant, c is the speed of light, G is the gravitational constant, m_{H} is the mass of hydrogen, Z is the number of protons, A is the number of nucleons, and M_{\odot} is the mass of the sun. This formula can be found in (Carroll & Ostlie 2006). More precisely, $M_{\text{Ch}} = 1.44M_{\odot}$.

Because neutron stars are supported by a neutron degeneracy pressure, the radius of a neutron star can be approximated as

$$R_{\text{ns}} \approx \frac{(18\pi)^{2/3}}{10} \frac{\hbar^2}{GM_{\text{ns}}^{1/3}} \left(\frac{1}{m_{\text{H}}} \right)^{8/3} \quad (2.2)$$

This formula can be found in (Carroll & Ostlie 2006). The canonical radius for neutron stars is ~ 10 km.

In these very dense environments, the protons and electrons in the neutron star form into neutrons through inverse β decay:

$$p^+ + e^- \rightarrow n + \nu_e. \quad (2.3)$$

But if a neutron star had a sufficiently large mass, the gravitational force would overpower the neutron degeneracy pressure and the object would collapse into a black hole. The maximum mass of a neutron star is unknown because it depends on the equation of state inside the star, but is commonly predicted to be $\sim 2.5M_{\odot}$. Recently, a pulsar with a mass of $\sim 2M_{\odot}$ was discovered (Demorest et al. 2010), constraining theories of the equation of state.

3 Types of pulsars (rotationally powered pulsars, magnetars, accretion powered pulsars,

2.6.2 Pulsar Evolution

- “Following this discovery, a theoretical understanding was soon developed in which the central pulsar generates a magnetized particle wind, whose ultrarelativistic electrons and positrons radiate synchrotron emission across the electromagnetic spectrum (Pacini & Salvati 1973, Rees & Gunn 1974). The pulsar has steadily released about a third of its total reservoir of 10^{50} ergs of rotational energy into its surrounding nebula over the last 950 years. This is in sharp contrast to shell-like SNRs, in which the dominant energy source is the 10^{51} ergs of kinetic energy released at the moment of the original SN explosion.” – Gaensler & Slane (2006)
- What is termination shock of PWNs.
- How is pulsar outflow accelerated at shock?

The simplest model of a pulsar is that it is a rotating dipole magnet. It is shown in Figure 2.5.

Find a plot of a rotating pulsar. The simplest rotating dipole model

The energy powering pulsars and PWNs is commonly believed to originate in rotational kinetic energy stored in the neutron star. Both the period P and the period derivative $\dot{P} = dP/dt$ can be directly observed for a pulsar and typically the pulsar is slowing down ($\dot{P} < 0$). We write the rotational kinetic energy as

$$E_{\text{rot}} = \frac{1}{2} I \Omega^2 \quad (2.4)$$

where $\omega = 2\pi/P$ and P is the period of rotation of the pulsar. We make the connection between the pulsar’s spin-down energy and the rotational kinetic energy as $\dot{E} = -dE_{\text{rot}}/dt$

The rotational kinetic energy in a pulsar can be written as

$$\dot{E} = 4\pi^2 I \dot{P} / P^2, \quad (2.5)$$

where I is the moment of inertia. For a uniform sphere,

$$I = \frac{2}{5}MR^2 \quad (2.6)$$

Pulsars are assumed to be uniform spheres with $R = 10 \text{ km}$ and $M = 1.4M_{\odot}$, which leads to a canonical moment of inertia of $I = 10^{45} \text{ gcm}^2$.

It is believed that as the pulsar spins down, this rotational energy is released as pulsed electromagnetic radiation and also as a wind of electrons and positrons accelerated in the magnetic field of the pulsar.

As the pulsar slows down, it releases the rotational kinetic energy

$$\dot{E} = -\frac{4\pi^2 I \dot{P}}{P^3} \quad (2.7)$$

where \dot{P} is the rate of decrease in the period of the pulsar.

Discuss uniform dipole model

We conventionally assume that the period and period derivative are related by the equation

$$\dot{\Omega} \propto \Omega^n \quad (2.8)$$

where $\Omega = 2\pi/P$, and n is the pulsar braking index.

- “though n has only been confidently measured for five pulsars, in each case falling in the range $2 \leq n \leq 3$ (Livingstone et al. (2007) and references therein).”
– Adam Van Etten’s thesis

- “The braking index is the power to which the slowdown in angular velocity occurs, and is defined as:

$$n = \frac{P\ddot{P}}{\dot{P}^2} + 2 \quad (2.9)$$

” – keogh_2010_search-pulsar

Equation 2.8 is a Bernoulli differential equation which can be integrated

to solve for time

$$T = \frac{P}{(n-1)|\dot{P}|} \left(1 - \left(\frac{P_0}{P} \right)^{(n-1)} \right) \quad (2.10)$$

- TODO: cite Manchester & Taylor 1977

$$\tau_c = P/2\dot{P} \quad (2.11)$$

- What is a typical moment of inertia, typical dE/dT
- What fraction of pulsar energy is released observationally

2.6.3 Pulsar Magnetosphere

2.6.4 Pulsar Wind Nebulae

- Discuss termination shock (i.e. section 3.3.2 of dalton_2011_identification-gamma-ray)
- The radius of the termination shock is

$$r_{ts} = \sqrt{\frac{\dot{E}}{\frac{4}{3}\pi P_{ISM}c}} \quad (2.12)$$

Discuss pulsar evolution “The Evolution and Structure of Pulsar Wind Nebulae”
– Bryan M. Gaensler and Patrick O. Slane

Describe Mattana’s work on PWNs: “On the evolution of the Gamma- and X-ray luminosities of Pulsar Wind Nebulae”

2.7 Modeling the Galactic Diffuse and Isotropic Gamma-ray Background

Include discussion of modeling, if time permitting

- Discuss the historical Observations of galactic diffuse emission
Mention how OSO-3 first detected the *gamma*-rays from the galaxy: Section 2.2.
- GALPROP model of diffuse emission. Reference: <http://arxiv.org/abs/1202.4039>
- Empirical Ring model of galactic diffuse emission.
- The isotropic background: <http://arxiv.org/abs/1002.3603>
- Galactic diffuse emission is primarily composed of ...
- Something about how great galprop is.
- Something about

2.8 Sources Detected by the Fermi The Large Area Telescope

- A variety of sources detected by the The Large Area Telescope:

2.8.1 The second *Fermi* catalog

The second *Fermi* catalog (2FGL) was a catalog by the LAT collaboration containing XXX Sources.

Describe Catalog

- Citation is Nolan et al. (2012)
- Source classification method
- Number of sources detected by the LAT
- Forward reference Chapter 3, which does a more thorough description of likelihood analysis method.
- Source classes/associations

2.8.2 The second *Fermi* pulsar catalog

The second *Fermi* pulsar catalog (2PC) is a ...

- Process of detecting Pulsars with the LAT
- Number of pulsars detected by the LAT

2.8.3 Pulsar wind nebula Detected by the The Large Area Telescope

Crab

Vela X

MSH 15-52

Dig up HESS reference of HESS J1514-59.

HESS J1825–137

HESS J1825–137 is a cool source

HESS Detection: HESS Energy dependent morphology: Aharonian et al. (2006a)

LAT Detection: Grondin et al. (2011)

HESS J1640–465

HESS J1640–465 is also cool.

HESS detection: Aharonian et al. (2006b) Fermi detection: Slane et al. (2010)

2FGL J1857+026

2FGL J1857+026 is another good source.

LAT detection: Rousseau et al. (2012)

1. <http://arxiv.org/pdf/1206.3324v1.pdf>

J1023

...

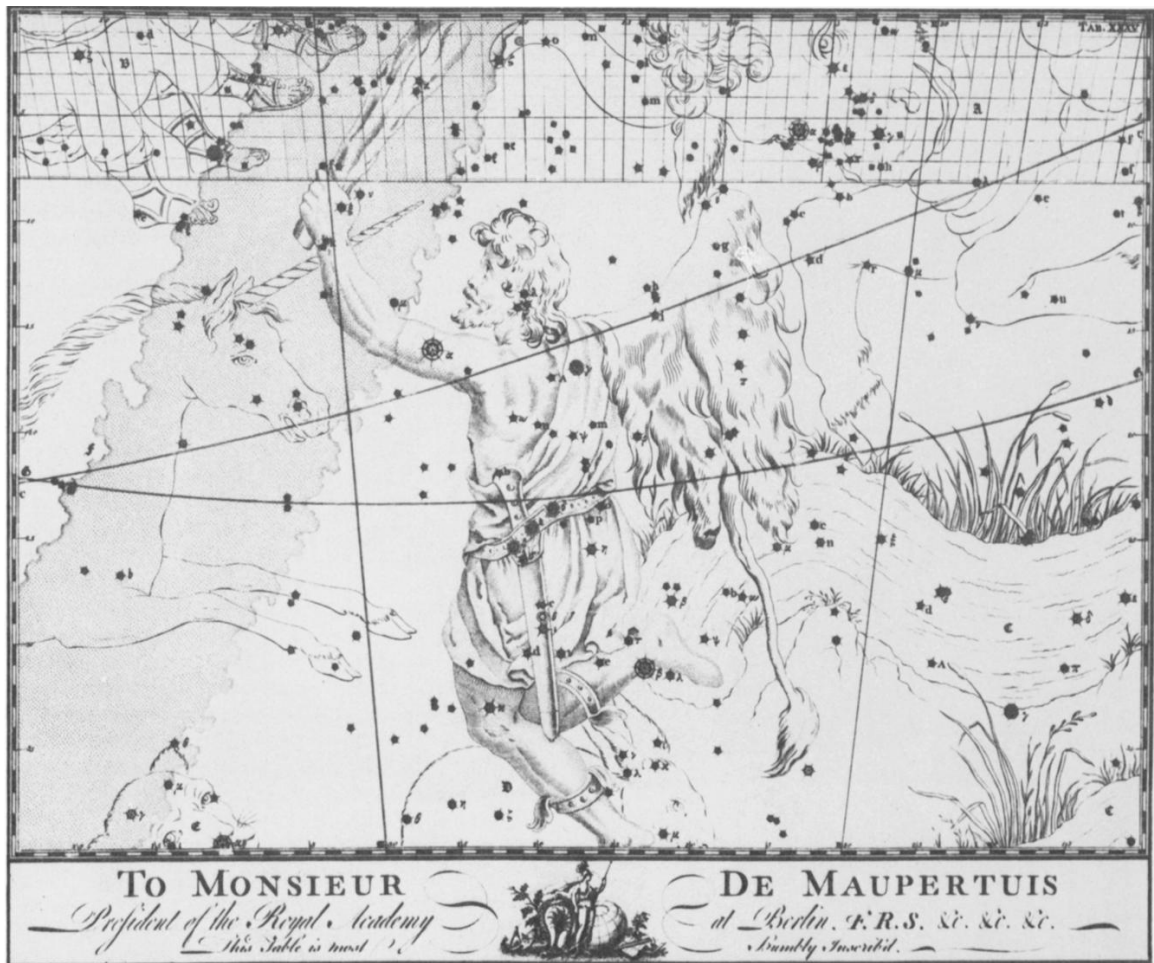


Figure 2.4: The Orion plate from Bevis' book *Uranographia Britannica*. The Crab nebula can be found on the horn of Taurus the Bull on the top of the figure and the source is marked by a cloudy symbol. This figure was reproduced from Ashworth (1981).

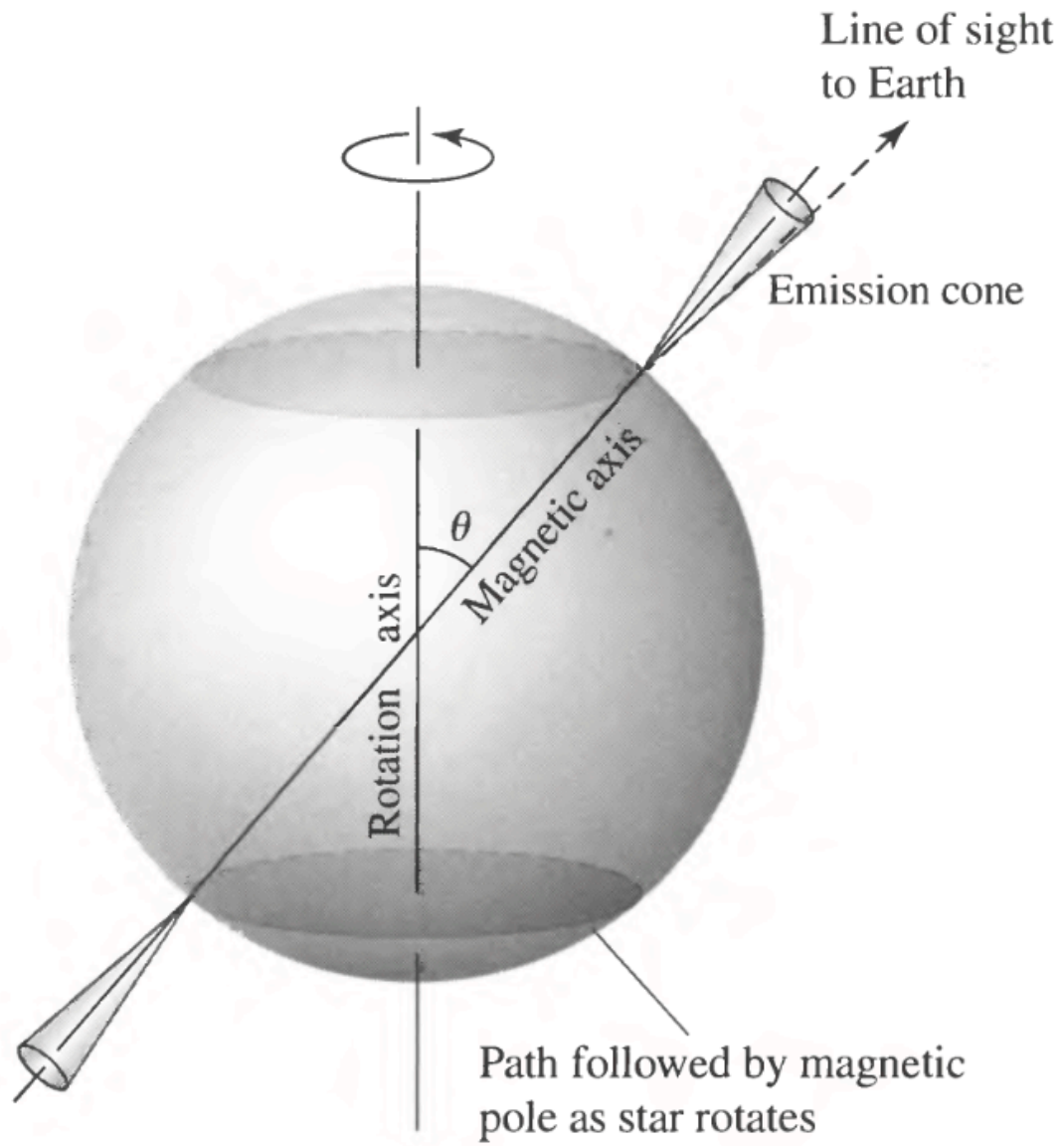


Figure 2.5: The simplest model of a pulsar. Figure from (Carroll & Ostlie 2006).

Chapter 3

Maximum-likelihood analysis of LAT data

In this chapter, we discuss maximum-likelihood analysis, the principle analysis method used to perform spectral and spatial analysis of LAT data. In Section 3.1, we discuss the reasons necessary for employing this analysis procedure compared to other simpler analysis methods. In Section 3.2, we describe the benefits of a maximum-likelihood analysis. In Section 3.3, we discuss the steps involved in defining a complete model of the sky, a necessary part of any likelihood analysis.

In Section 3.5, we discuss the standard implementation of binned maximum likelihood in the LAT Science Tools and in particular the tool `gtlike`. In Section 3.6, we then discuss the `pointlike` package, an alternate package for maximum-likelihood analysis of LAT data. We discuss the similarities and differences between `pointlike` and `gtlike`.

In the next chapter (Chapter 4), we will discuss the addition of capability into `pointlike` for studying spatially-extended sources and the analysis method which will be used in this paper to study spatially-extended sources.

We note that much of the notation and formulation of likelihood analysis in this chapter follows Kerr (2010).

3.1 Motivations for Maximum-Likelihood Analysis of Gamma-ray Data

Traditionally, spectral and spatial analysis of astrophysical data relies on a process known as aperture photometry. In this process, a source in the data is analyzed by directly measuring the number of photons coming from the object. This process is done by measuring the counts within a given radius of the source and subtracting from it a background level estimated from a nearby region. Often, the source's flux is calibrated by measurements of nearby objects with known fluxes. Otherwise, the flux can be obtained from by dividing the number of counts from the source by the telescope's size, the observation time, and the telescope's conversion efficiency.

Similarly, for faint sources the statistical significance of the detection can be obtained from the Poisson nature of the data. For TeV experiments such as H.E.S.S., this analysis method is described in Li & Ma (1983).

Unfortunately, this simpler analysis method is inadequate for dealing with the complexities introduced in analyzing LAT data.

Most importantly, aperture photometry assumed that the background is isotropic so that the background level below the source can be estimated from nearby regions. As was discussed in Section 2.7, the Galactic diffuse emission is highly anisotropic, rendering this assumption invalid.

In addition, this method is not optimal due to the high density of sources detected in the Gamma-ray sky. 2FGL reported on the detection of 1873 sources, which corresponds to an average source spacing of $\sim 5^\circ$. But within the inner 45° of the galactic plane in longitude and 0.5° of the galactic plane in latitude, there are 73 sources, corresponding to a source density of ~ 1 source per square degree. The aperture photometry method is unable to effectively fit multiple sources when the tails of the PSF overlap and furthermore make background estimation problematic.

Finally, this method is suboptimal due to the large energy range of LAT observations. A typical spectral analysis studies a source from an energy of 100 MeV to energies above 100 GeV. Similarly, as was shown in , the PSF of the LAT is rather broad ($\gtrsim 1^\circ$) at low energy and much narrower ($\sim 0.1^\circ$) at higher energies. Therefore,

what
section
dis-
cusses
en-
ergy

there is a much higher sensitivity to the higher energy photons coming from a source. But simple aperture photometry method would ignore this improvement by weighting each photon equally.

3.2 Description of Maximum-Likelihood Analysis

The field of γ -ray astrophysics has generally found maximum-likelihood to be a dependable method to avoid the issues discussed above. The term likelihood was first introduced by Fisher (1925). Maximum-likelihood was applied to photon-counting experiments in the context of astrophysics by Cash (1979). Mattox et al. (1996) described the maximum-likelihood analysis framework developed to analyze EGRET data.

In the formulation, one relies upon primarily upon the likelihood function. The likelihood, denoted \mathcal{L} , is quite simply the probability of obtaining the observed data given an assumed model:

$$\mathcal{L} = P(\text{data}|\text{model}) \quad (3.1)$$

Section 3.3 will provide describe the components that go into a model of the data.

Generally, a model of the sky depends upon a list of parameters that we denote as $\vec{\lambda}$. Therefore, the likelihood function itself becomes a function of the parameters of the model:

$$\mathcal{L} = \mathcal{L}(\vec{\lambda}) \quad (3.2)$$

The term maximum-likelihood refers to the fact that the best-fit parameters of a model can be estimated by maximizing the likelihood function.

What are the benefits of maximum likelihood

Describe Wilk's Theorem and its application to parameter error estimation

3.3 Defining a Model of the Sources in the Sky

In order to perform a maximum-likelihood analysis, one requires a parameterized model of the sky. A model of the sky is composed of a set of γ -ray sources, each

characterized by its photon flux density $\mathcal{F}(E, t, \vec{\Omega}|\vec{\lambda})$. This represents the number of photons emitted per unit energy, per unit time, per units solid angle at a given energy, time, and position in the sky. In the Centimetre-Gram-Second System of Units (CGS), it has units of $\text{ph cm}^{-2}\text{s}^{-1}\text{erg}^{-1}\text{sr}^{-1}$.

Often, the spatial and spectral part of the source model are separable and independent of time. When that is the case, we like to write the source model as

$$\mathcal{F}(E, t, \vec{\Omega}|\vec{\lambda}) = \frac{dN}{dE} \times \text{PDF}(\vec{\Omega}). \quad (3.3)$$

Here, $\frac{dN}{dE}$ is only a function of energy and $\text{PDF}(\vec{\Omega})$ is only a function of position ($\vec{\Omega}$). In this formulation, some of the model parameters $\vec{\lambda}$ are taken by the $\frac{dN}{dE}$ function and some by the $\text{PDF}(\vec{\Omega})$ function. In CGS, $\frac{dN}{dE}$ is in units of $\text{ph cm}^{-2}\text{s}^{-1}\text{erg}^{-1}$.

The spectrum $\frac{dN}{dE}$ is typically modeled by simple geometric functions. The most popular spectral model is a power law (PL):

$$\frac{dN}{dE} = N_0 \left(\frac{E}{E_0} \right)^{-\gamma} \quad (3.4)$$

Here, $\frac{dN}{dE}$ is a function of energy and also for the two model parameters (the prefactor N_0 and the spectral index γ). The parameter E_0 is often called the energy scale or the pivot energy and is not considered a model parameter.

Another common spectral model is the broken-power law (BPL) spectral model

$$\frac{dN}{dE} = N_0 \times \begin{cases} (E/E_b)^{-\gamma_1} & \text{if } E < E_b \\ (E/E_b)^{-\gamma_2} & \text{if } E \geq E_b \end{cases} \quad (3.5)$$

This model represents a powerlaw with an index of γ_1 which has a break at energy E_b to having an index of γ_2 .

Finally, the exponentially-cutoff power law (ECPL) spectral model is often used to model the γ -ray emission from pulsars:

$$\frac{dN}{dE} = N_0 \left(\frac{E}{E_0} \right)^{-\gamma} \exp \left(-\frac{E}{E_c} \right). \quad (3.6)$$

For energies much below E_c , the ECPL is a PL with spectral index γ . For energies much larger than E_c , the ECPL exponentially decreases.

PDF represents the spatial distribution of the emission. It is traditionally normalized as though it was a probability:

$$\int d\Omega \text{PDF}(\vec{\Omega}). \quad (3.7)$$

Therefore, in CGS PDF has units of sr^{-1} . For a point-like source at a position $\vec{\Omega}'$, the spatial model is:

$$\text{PDF}(\vec{\Omega}) = \delta(\vec{\Omega} - \vec{\Omega}') \quad (3.8)$$

and is a function of the position of the source. Example spatial models for spatially-extended sources will be presented in section XXXXX.

This formulation assumed that the source models are not time dependent. This is traditionally because it is difficult to find simple parameterized models to fit the time behavior of a variable source. Instead, the typical strategy to fit variable sources is to divide a large range of time into multiple smaller time intervals and to perform multiple likelihood fits in each time range.

In some situations, the spatial and spectral part of a source do not nicely decouple. An example of this could be supernova remnants (SNRs) which could show a spectral variation across the source. Katsuta et al. (2012) and Hewitt et al. (2012) have simplified this problem by a simple method which has been adopted to study this kind of source.

FINISH DISCUSSION

In situations where spatial and spectral components couple, typical to make multiple spatial templates, each with an independent spectra (e.g. the Puppis A paper's fitting multiple hemispheres).

Discuss how diffuse background is more complicated and requires a mapcube.

WHAT
SEC-
TION
DE-
SCRIBES
EX-
TENDED
SOURCE
PDFs

3.4 The LAT Instrument Response Functions

The performance of the LAT is composed of two effects. The efficiency of the LAT refers to its ability to reconstruct a photon which comes into the detect. The dispersion of the LAT refers to the probability of misreconstructing an event.

The efficiency is typically called the effective area. We write it as $\epsilon(E, t, \vec{\Omega})$. It is a function of energy, time, and solid angle (SA). It is measured in units of area (cm^2).

LINK TO [arXiv:1206.1896](https://arxiv.org/abs/1206.1896) for MORE THOUROUGH DISCUSSION OF EFFECTIVE AREA

DISCUSS HOW EFFECTIVE AREA IS A FUNCTION OF DIFFERENT THINGS

The dispersion is the probability of a photon with true energy E and incoming direction $\vec{\Omega}$ at time t being reconstructed to have an energy E' , an incoming direction $\vec{\Omega}'$ at a time t' . The dispersion is written as $P(E', t', \vec{\Omega}' | E, t, \vec{\Omega})$. It represents a probability and is therefore normalized such that

$$\int \int \int dE d\Omega dt P(E', t', \vec{\Omega}' | E, t, \vec{\Omega}) = 1 \quad (3.9)$$

What is the range of the integrals

Therefore, $P(E', t', \vec{\Omega}' | E, t, \vec{\Omega})$ has units of $1/\text{energy}/\text{SA}/\text{time}$

We assume these two factors to decouple and write the LAT's instrument response as

$$R(E', \vec{\Omega}', t' | E, \vec{\Omega}, t) = \epsilon(E, t, \vec{\Omega}) P(E', t', \vec{\Omega}' | E, t, \vec{\Omega}) \quad (3.10)$$

Therefore, the instrument response has units of $\text{area}/\text{energy}/\text{SA}/\text{time}$

The convolution of the flux of a model with the instrument response produces the expected counts per unit energy/time/SA begin reconstructed to have an energy E' at a position $\vec{\Omega}'$ and at a time t' :

$$\tau(E', \vec{\Omega}', t' | \vec{\lambda}) = \int \int \int dE d\Omega dt \mathcal{F}(E, t, \vec{\Omega} | \vec{\lambda}) R(E', \vec{\Omega}', t' | E, \vec{\Omega}, t) \quad (3.11)$$

Here, this integral is performed over all true energies, SAs, and times for which the source model has support.

For LAT analysis, we conventionally make the simplifying assumption that the energy, spatial, and time dispersion decouple:

$$P(E', t', \vec{\Omega}' | E, t, \vec{\Omega}) = \text{PSF}(\vec{\Omega}' | E, \vec{\Omega}) \times E_{\text{disp}}(E' | E) \times T_{\text{disp}}(t' | t) \quad (3.12)$$

Here, PSF is the point-spread function and represents ...

BETTER DISCUSSION OF PSF OF THE LAT, WHAT ITS SCALE IS...

E_{disp} represents the energy dispersion of the LAT. The energy dispersion of the LAT is a function of both the incident energy and incident angle of the photon. It varies from $\sim 5\%$ to 20% , degrading at lower energies due to energy losses in the tracker and at higher energy due to electromagnetic shower losses outside the calorimeter. Similarly, it improves for photons with higher incident angles that are allowed a longer path through the calorimeter (Ackermann et al. 2012).

For sources with smoothly-varying spectra, the effects of ignoring the inherent energy dispersion of the LAT are typically small. Ackermann et al. (2012) performed a monte carlo simulation to show that for power-law point-like sources, the bias introduced by ignoring energy dispersion was on the level of a few percent. Therefore, energy dispersion is typically ignored for standard likelihood analysis:

$$E_{\text{disp}} = \delta(E - E') \quad (3.13)$$

We caution that for analysis of sources extended to energies below 100 MeV and for sources expected to have spectra that do not smoothly vary, the effects of energy dispersion could be more severe.

- T_{disp} is the time dispersion.
- _____
- The timing dispersion is $< 10 \mu\text{s}$ Atwood et al. (2009)
- WRITE ENERGY DISPERSION AS A DELTA FUNCTION

Why
dis-
card
time
dis-
per-
sion

Therefore, the instrument response is typically approximated as

FINISH

$$R(E', \vec{\Omega}', t' | E, \vec{\Omega},) = \epsilon(E, t', \vec{\Omega}) \text{PSF}(\vec{\Omega}' | E, \vec{\Omega}) \quad (3.14)$$

The expected count rate is then typically integrated over time to compute the total counts. Assuming that the source model is time independent, we get:

$$\tau(E', \vec{\Omega}' | \vec{\lambda}) = \int d\Omega \mathcal{F}(E, \vec{\Omega} | \vec{\lambda}) \left(\int dt \epsilon(E, t, \vec{\Omega}) \right) \text{PSF}(\vec{\Omega}' | E, \vec{\Omega}) \quad (3.15)$$

This equation essentially says that the counts expected by the LAT for the particular model is the product of the source's flux with the effective area and then convolved with the point-spread function.

Figure out how the θ dependence of the IRFs factors into this calculation

3.5 Binned Maximum-Likelihood of LAT Data with the Science Tools

- For a standard LAT analysis, we perform a binned maximum-likelihood analysis:
- In the standard science tools, the data is binned in position and energy. and integrated in energy.
- For time-series analysis, typically a time-summed analysis is performed successivly in multiple time bins.
- The likelihood comes from a sum over each bin
- The likelihood is defined as

$$\mathcal{L} = \prod_j \frac{\theta_j^{n_j} e^{-\theta_j}}{n_j!} \quad (3.16)$$

– Here, j is a sum over position/energy bins.

- θ_j is the counts predicted by the model, which is defined following the discussion in Section 3.3.
- n_j are the observed counts in the spatial/energy bin j
- The model counts are computed by integrating the differential counts defined in Equation 3.11 over the energy bin:

$$\theta_{ij} = \int_j dE d\Omega dt \tau(E, \vec{\Omega}, t | \vec{\lambda}_i) \quad (3.17)$$

Here, j represents the integral over the j th position/energy bin, i represents the i th source, and $\vec{\lambda}_i$ refers to the parameters defining the i th source. The total model counts is computed by summing over all sources:

$$\theta_j = \sum_i \theta_{ij} \quad (3.18)$$

- In the standard *Fermi* science tools, the binning of photons over position in the sky and energy to compute n_j is done with `gtbin`.
- In the standard *Fermi* science tools, the model counts θ_j are computed in several steps . . .
- The instrument response is computed with a combination of `gtltcube`, `gtexpcube`.
- Convert a model of the sky into model predicted counts
- poisson likelihood
- Particular implementation of maximum likelihood analysis
- Describe `gtbin`, `gtselect`, `gtlike`

Write Section or Perform simple MC Simulation to demonstrate significance of detection

3.6 The Alternate Maximum-Likelihood Package `pointlike`

- Developed for Speed
- Sparse Matrices,
- Methods for computing integral model counts.

Chapter 4

Analysis of Spatially Extended LAT Sources

This chapter is based the first part of the the paper “Search for Spatially Extended Fermi-LAT Sources Using Two Years of Data” by Lande et al. 2012 ApJ, 756, 5

4.1 Analysis Method

4.2 Validation of the TS Distribution

4.3 Extended Source Detection Threshold

4.4 Testing Against Source Confusion

4.5 Test of 2LAC Sources

4.6 Systematic Errors on Extension

Chapter 5

Search for Spatially-extended LAT Sources

This chapter is based the second part of the the paper “Search for Spatially Extended Fermi-LAT Sources Using Two Years of Data” by Lande et al. 2012 ApJ, 756, 5

5.1 Extended Source Search Method

5.2 New Extended Sources

5.3 Discussion

Chapter 6

Search for Pulsar Wind Nebulae associated with Gamma-loud Pulsars

This chapter is based on work from 2PC. GET REFERENCE HERE.

6.1 Off-peak Phase Selection

6.2 Off-peak Analysis Method

6.3 Off-peak Results

6.4 Off-Peak Individual Source Discussion

Chapter 7

Search for Pulsar Wind Nebulae associated with TeV Pulsars

Notes

- Only include sources classified as PWN in TeVCat.
- Always model LAT Pulsar in the background (???)

7.1 List of Candidates

7.2 Analysis Method

7.3 Sources Detected

Chapter 8

Search for Pulsar Wind Nebulae associated with High \dot{E} Pulsars

Chapter 9

Population Study of The Large Area Telescope (LAT)-detected Pulsar wind nebula (PWN)

Chapter 10

Future Work (or Outlook)??

What would make good future work. Something about CTA population study, something about improved modeling like HESS J1825, something about better PSF

Bibliography

- Ackermann, M., Ajello, M., Albert, A., et al. 2012, ApJS, 203, 4
- Aharonian, F., Akhperjanian, A. G., Bazer-Bachi, A. R., et al. 2006a, A&A, 460, 365
- . 2006b, ApJ, 636, 777
- Arnold, J. R., Metzger, A. E., Anderson, E. C., & van Dilla, M. A. 1962, J. Geophys. Res., 67, 4878
- Ashworth, William B., J. 1981, Proceedings of the American Philosophical Society, 125, pp. 52
- Atwood, W. B., Abdo, A. A., Ackermann, M., et al. 2009, ApJ, 697, 1071
- Baum, W. A., Johnson, F. S., Oberly, J. J., et al. 1946, Phys. Rev., 70, 781
- Bertsch, D. L., Brazier, K. T. S., Fichtel, C. E., et al. 1992, Nature, 357, 306
- Bignami, G. F., Boella, G., Burger, J. J., et al. 1975, Space Science Instrumentation, 1, 245
- Bradt, H., Rappaport, S., & Mayer, W. 1969, Nature, 222, 728
- Browning, R., Ramsden, D., & Wright, P. J. 1971, Nature Physical Science, 232, 99
- Burnight, T. 1949, Phys. Rev, 76, 19
- Carroll, B. W., & Ostlie, D. A. 2006, An Introduction to Modern Astrophysics, 2nd edn. (Benjamin Cummings)

- Cash, W. 1979, *ApJ*, 228, 939
- Chandrasekhar, S. 1931, *ApJ*, 74, 81
- Cocke, W. J., Disney, M. J., & Taylor, D. J. 1969, *Nature*, 221, 525
- Critchfield, C. L., Ney, E. P., & Oleksa, S. 1952, *Physical Review*, 85, 461
- Demorest, P. B., Pennucci, T., Ransom, S. M., Roberts, M. S. E., & Hessels, J. W. T. 2010, *Nature*, 467, 1081
- Feenberg, E., & Primakoff, H. 1948, *Phys. Rev.*, 73, 449
- Fichtel, C. E., Hartman, R. C., Kniffen, D. A., et al. 1975, *ApJ*, 198, 163
- Fisher, R. A. 1925, *Statistical Methods for Research Workers* (Edinburgh: Oliver and Boyd)
- Fritz, G., Henry, R. C., Meekins, J. F., Chubb, T. A., & Friedman, H. 1969, *Science*, 164, 709
- Gaensler, B. M., & Slane, P. O. 2006, *ARA&A*, 44, 17
- Gold, T. 1968, *Nature*, 218, 731
- Grondin, M.-H., Funk, S., Lemoine-Goumard, M., et al. 2011, *ApJ*, 738, 42
- Hayakawa, S. 1952, *Progress of Theoretical Physics*, 8, 571
- Herschel, W. 1800, *Philosophical Transactions of the Royal Society of London*, 90, pp. 284
- Hewish, A., Bell, S. J., Pilkington, J. D. H., Scott, P. F., & Collins, R. A. 1968, *Nature*, 217, 709
- Hewitt, J., Grondin, M.-H., Lemoine-Goumard, M., et al. 2012
- Hulsizer, R. I., & Rossi, B. 1948, *Phys. Rev.*, 73, 1402

- Hutchinson, G. 1952, *Philosophical Magazine Series* 7, 43, 847
- Jansky, K. 1933, *Proceedings of the Institute of Radio Engineers*, 21, 1387
- Katsuta, J., Uchiyama, Y., Tanaka, T., et al. 2012
- Kerr, M. 2010, PhD thesis, University of Washington
- Kniffen, D. A., & Fichtel, C. E. 1970, *ApJ*, 161, L157
- Kraushaar, W., Clark, G. W., Garmire, G., et al. 1965, *ApJ*, 141, 845
- Kraushaar, W. L., Clark, G. W., Garmire, G. P., et al. 1972, *ApJ*, 177, 341
- Large, M. I., Vaughan, A. E., & Mills, B. Y. 1968, *Nature*, 220, 340
- Li, T.-P., & Ma, Y.-Q. 1983, *ApJ*, 272, 317
- Mattox, J. R., Bertsch, D. L., Fichtel, C. E., et al. 1992, *ApJ*, 401, L23
- Mattox, J. R., Bertsch, D. L., Chiang, J., et al. 1996, *ApJ*, 461, 396
- Mayer-Hasselwander, H. A., Kanbach, G., Bennett, K., et al. 1982, *A&A*, 105, 164
- McK Mahille, J., Schild, R., Wendorf, F., & Brenner, R. 2007, *African Skies*, 11, 2
- Morrison, P. 1958, *Il Nuovo Cimento*, 7, 858
- Nolan, P. L., Abdo, A. A., Ackermann, M., et al. 2012, *ApJS*, 199, 31
- Pacini, F. 1967, *Nature*, 216, 567
- . 1968, *Nature*, 219, 145
- Rousseau, R., Grondin, M.-H., Van Etten, A., et al. 2012, *A&A*, 544, A3
- Slane, P., Castro, D., Funk, S., et al. 2010, *The Astrophysical Journal*, 720, 266
- Staelin, D. H., & Reifstein, III, E. C. 1968, *Science*, 162, 1481
- Swanenburg, B. N., Hermsen, W., Bennett, K., et al. 1978, *Nature*, 275, 298

Swanenburg, B. N., Bennett, K., Bignami, G. F., et al. 1981, ApJ, 243, L69

Thompson, D. J., Fichtel, C. E., Hartman, R. C., Kniffen, D. A., & Lamb, R. C.
1977a, ApJ, 213, 252

Thompson, D. J., Fichtel, C. E., Kniffen, D. A., & Ogelman, H. B. 1977b, ApJ, 214,
L17